Chaotic ionization of a stationary electron state via a phase space turnstile

Korana Burke, Kevin A. Mitchell, Shuzhen Ye, and F. Barry Dunning

Chaotic Ionization of a Stationary Electron State via a Phase Space Turnstile

Korana Burke

Department of Physics, University of California, Davis, CA, 95616, USA

Kevin A. Mitchell

School of Natural Sciences, University of California, Merced, CA 95344, USA

Shuzhen Ye and F. Barry Dunning

Department of Physics and Astronomy and the Rice Quantum Institute, Rice University, Houston, Texas 77005, USA

The ionization of a highly excited Rydberg atom subjected to a periodic sequence of electric field impulses, or "kicks", is chaotic. We focus on the dynamics of a single kicking period in order to isolate the ionization mechanism. Potassium Rydberg atoms, prepared in a quasi-one-dimensional state, are exposed to a sequence of ionization kicks, and the total fraction of ionized atoms is then measured. These experimental data are compared to a one-dimensional classical model. The classical analysis reveals that the ionization process is governed by a phase space turnstile—a geometric structure associated with chaotic transport in diverse systems. The turnstile geometry is reflected in the experimental data. Previous work explored the dependence of the turnstile geometry on the kicking period. The present work explores the dependence on the kicking strength. In particular, increasing the kicking strength allows us to observe the stretching of the turnstile lobe as it penetrates the region of phase space occupied by the electronic state, leading to a sharp rise in the total ionization fraction. This work thus highlights the importance of phase space geometry in organizing chaotic transport in atomic systems.

I. INTRODUCTION

Many physical systems display complex chaotic behavior [1, 2]. Such systems span a broad range of length scales and include global weather patterns [3], mixing of fluids [4–6], and firing of neurons [7]. One mesoscale system that has been used recently to study non-linear dynamics and chaos is the kicked Rydberg atom[8–11], i.e., a high-n atomic state that is subject to a series of electric field pulses (termed half-cycle pulses, HCPs) with durations $\tau_k \ll T_n$, where T_n is the electron Kepler period. In this regime each HCP simply delivers an impulsive momentum transfer, or "kick", to the excited electron given by $\Delta \boldsymbol{p} = \int \boldsymbol{F}(t)dt$, where $\boldsymbol{F}(t)$ is the force exerted on the electron as a result of the applied HCP. (Atomic units are used throughout unless otherwise noted.) Atoms subject to a series of such kicks exhibit a plethora of rich dynamics. For example, application of a periodic series of unidirectional kicks to a quasi-one-dimensional (quasi-1D) Rydberg atom that are directed towards the nucleus along the atomic axis leads to a mixed phase space containing a series of stable islands that are embedded in a chaotic sea. Such islands have been used to trap electronic wave packets and transport them to different regions of phase space [8, 11]. In contrast, application of a periodic series of unidirectional kicks away from the nucleus leads to fully chaotic behavior, with no islands.

This paper focuses on the geometric structures present in the phase space of a Rydberg atom subject to external electric field pulses of *alternating* sign, i.e. alternating between kicks toward and away from the nucleus. Earlier work indicated that ionization in this system is controlled by a geometric structure of phase space called a turnstile, which promotes electrons from bound to ionized states during one kicking cycle [10, 12]. (For another example of turnstile-mediated ionization see Refs. [13–15].) Those electrons whose initial phase points reside within the turnstile ionize after one kicking cycle, whereas those with phase points lying outside the turnstile may ionize only after application of additional kicking cycles.

The important role played by the turnstile in chaotic ionization was highlighted in a recent series of experiments using quasi-1D, $n \sim 306$ and $n \sim 350$, Rydberg atoms in which an HCP was used to create an electronic wave packet that exhibited transient localization in phase space [10]. By controlling the overlap between the wave packet and the turnstile, it was shown that when the overlap was large, a sizable fraction of the Rydberg atoms was ionized, whereas when the overlap was small, the majority of atoms survived. In the present work we demonstrate a more direct test of the turnstile's role; an initial quasi-1D *stationary* Rydberg state is employed. Furthermore unlike [10] in which only the duration of the kicking cycle was varied, here we vary both the duration and the kick *strength*. Varying the kick strength allows us to probe the transition from no ionization to more than 50% ionization. The experimental results are analyzed with the aid of a one-dimensional classical theory that predicts characteristic features seen in the data. These features are explained in terms of the geometry of the turnstile, further emphasizing the importance of phase space geometry in determining the behavior of chaotic atomic systems.

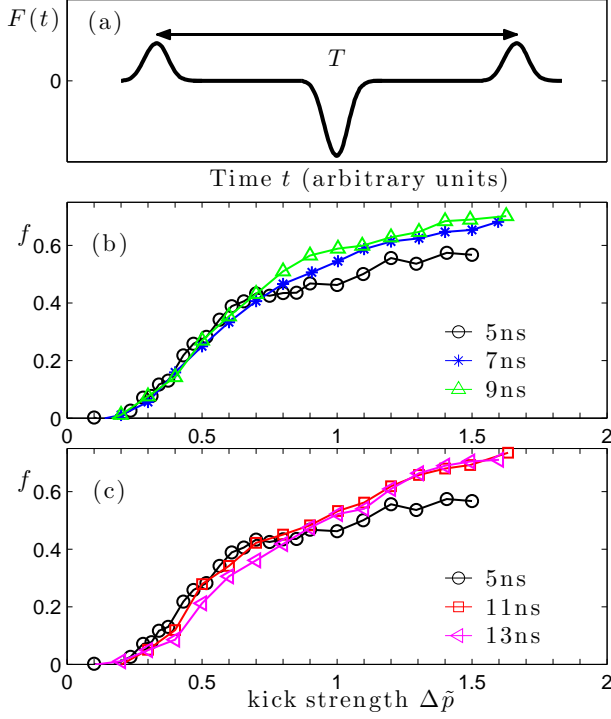This paper is organized as follows: Section II describes

FIG. 1: Experimentally measured ionization fractions for quasi-1D $n \sim 306$ Rydberg atoms subject to the sequence of kicks shown in figure (a) as a function of kick strength $\Delta\tilde{p}$ for the values of the periodic time T indicated.
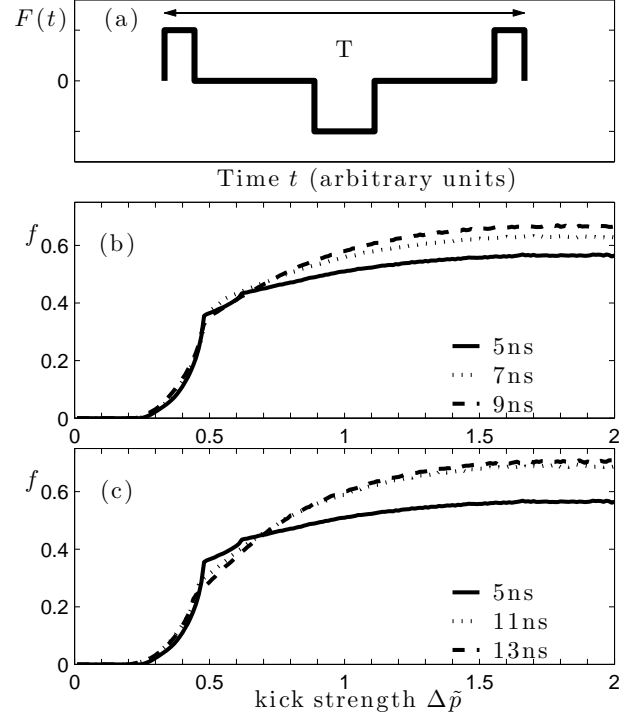

FIG. 2: Classical 1D simulations of ionization fractions for quasi-1D $n \sim 306$ Rydberg atoms subject to the sequence of kicks shown in figure (a) as a function of kick strength $\Delta\tilde{p}$ for the values of the periodic time T indicated.

the trends observed in experimental results; Section III details the results observed in the one-dimensional numerical simulations of the experiment; Section IV introduces the phase space geometry that governs the dynamics of this system; Section V details how the geometric structure of phase space explains the signatures observed in both experimental and numerical results.

II. EXPERIMENTAL RESULTS

The quasi-1D atoms studied here were prepared by photoexciting ground state potassium atoms to selected $n \sim 306$ red-shifted Stark states in the presence of a weak ($\sim 400~\mu$V cm^{-1}) dc field. See Ref. [11] for details. The atoms were then subject to the three alternating positive and negative kicks in Fig. 1a; a positive kick is directed away from the nucleus, and a negative kick is directed toward the nucleus. The number of atoms that survive the three kicks was measured by selective field ionization. Measurements in which no kicks were applied were taken at routine intervals during data acquisition to monitor the number of Rydberg atoms initially created. This allowed the fraction f of atoms ionized by the kick sequence to be determined.

Figures 1b and 1c record the measured ionization fraction f as a function of kick strength $\Delta\tilde{p}$ for values of the kicking period T ranging from 5 ns (the smallest that

could be achieved experimentally) to 13 ns. (Tildes are used to denote scaled atomic units $\tilde{r} = r/n^2$, $\tilde{t} = t/n^3$, $\tilde{E} = n^2 E$, $\Delta\tilde{p} = n\Delta p$.) Focusing on the 5ns data in Fig. 1b, the ionization fraction remains close to zero for weak kicks up to $\Delta\tilde{p}_0 \lesssim 0.2$. At $\Delta\tilde{p}_0 \approx 0.2$ the ionization fraction begins to increase rapidly until it reaches a "shoulder" at $\Delta\tilde{p}_{\text{shoulder}} \approx 0.6$ after which it grows more slowly. All three data series ($T = 5, 7, 9$ ns) in Fig. 1b are nearly identical up to this shoulder after which they separate and distinguish themselves: the larger the T value, the larger the ionization fraction f. Figure 1c repeats the $T = 5$ns data, for reference, and compares it to the $T = 11$ns and 13ns data. The initial rise of the 11ns and 13ns data can now be distinguished from the 5ns data. These two curves are initially below the 5ns data but then cross over it at about $\Delta\tilde{p} \approx 0.8$, remaining above it thereafter.

As will next be discussed, these experimental observations are in good agreement with one-dimensional theory, and the experimental features can be naturally explained within the context of the phase-space turnstile geometry.

III. NUMERICAL RESULTS

We adopt a classical one-dimensional hydrogenic model in which the electron is confined to move along a half line whose origin is at the nucleus. Time evolution

of this system is governed by the Hamiltonian

$$\tilde{H}(\tilde{r}, \tilde{p}_r) = \frac{\tilde{p}_r^2}{2} - \frac{1}{\tilde{r}} + \tilde{r}\tilde{F}(\tilde{t}), \qquad (1)$$

where $\tilde{r}$ and $\tilde{p}_r$ are electron position and momentum, respectively, and $\tilde{F}(\tilde{t})$ represents the electric field forcing. Recall that *tilde* denotes scaled atomic units. In these units the initial Rydberg state of the electron is represented by the stationary classical distribution along the energy shell $\tilde{E} = -1/2$. We model the experimental pulses with square wave pulses shown in Fig. 2a. After the application of these pulses to the initial Rydberg state we calculate the final electron energy distribution. The ionization fraction is determined as the fraction of electrons that acquire a positive energy.

Ionization fractions obtained in this manner are shown in Fig. 2b and Fig. 2c as a function of kick strength $\Delta\tilde{p}$ for the same values of the kicking period T as in Fig. 1. Despite the relatively simple model employed here, the behavior of the ionization fraction is in good agreement with the experimental data, and it displays many of the same features. For small values of $\Delta\tilde{p} \lesssim 0.3$ the ionization fraction is almost zero and only rises slowly with increasing $\Delta\tilde{p}$. At $\Delta\tilde{p}_0 \approx 0.25$, however, the ionization fraction begins to rise rapidly. For small values of T this rapid rise quickly terminates and transitions to a near "plateau" region where the ionization fraction increases much more slowly, this transition introducing a "shoulder" in the ionization curve at $\Delta\tilde{p}_{\text{shoulder}} \approx 0.5$. As T increases this shoulder disappears (Fig. 2c) and the ionization fraction increases much more uniformly with increasing kick strength. Nonetheless, for kick strengths $\Delta\tilde{p}_{\text{shoulder}} \lesssim 0.5$, the initial rise in the ionization fraction is largely independent of kicking period.

IV. PHASE SPACE GEOMETRY

The behavior of the ionization fraction f as a function of $\Delta\tilde{p}$ and T as discussed in Sections II and III can be readily explained by appealing to the geometry of the phase space turnstile, which is responsible for promoting the electron from a bound to an ionized state. Our main motivation for this paper is to understand the mechanism of chaotic ionization under a periodic driving force. The experimental pulse sequence in Fig. 1a was chosen to isolate one period of this driving. Therefore, here we consider the pulse sequence in Fig. 2a to be a part of an infinite pulse train in Fig. 3a. Instead of recording full electron orbits, we use the Poincaré return map $(\tilde{r}, \tilde{p}_r) \mapsto (\tilde{r}', \tilde{p}_r')$ that takes the electron's initial position and momentum and returns their values one kicking period T later. One period is marked by the thick red line in Fig. 3a. We define the time origin of the map as half way through the positive kick because this makes the map symmetric under time reversal.

The point $(\tilde{r}, \tilde{p}_r) = (\infty, 0)$ is an unstable fixed point of the electron dynamics. The stable and unstable man-
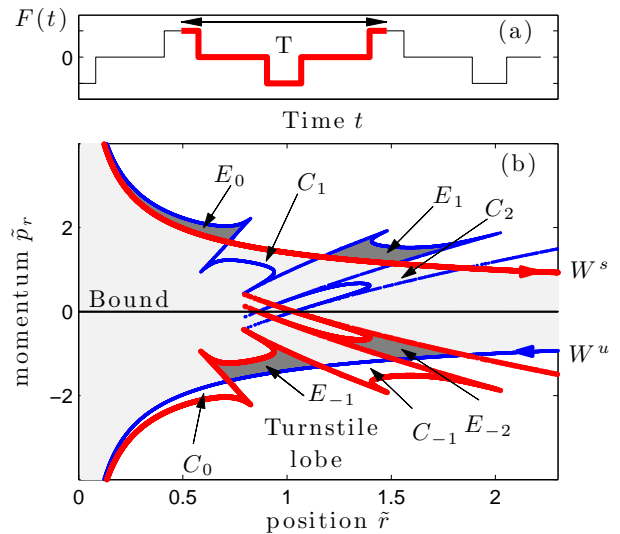

FIG. 3: (a) Periodic kicking used to compute the homoclinic tangle shown in the main figure (b). The thick red (thin blue) lines denote the stable (unstable) manifolds $W^s(W^u)$. The axes are labeled in scaled units.

ifolds attached to this unstable fixed point are shown in Fig. 3b. The stable manifold W^s (the thick red line) is a curve that contains those points that asymptotically converge onto the fixed point at infinity in the forward time direction [1]. Similarly, the unstable manifold W^u (the thin blue line) is a curve that contains those points that asymptotically converge onto the fixed point in the negative time direction. The stable and unstable manifolds together form an intricate pattern in phase space called a homoclinic tangle. The homoclinic tangle divides the phase space into an inner resonance zone (which we call the bound region) and an outer ionized zone. (The system parameters used in creating the homoclinic tangle shown in Fig. 3b are chosen for pedagogical reasons and do not correspond to parameters used to generate experimental or numerical results.)

The stable and unstable manifolds together define regions of phase space called lobes whose dynamics govern the time evolution in this system. Lobes fall into two categories: escape lobes, E_n, and capture lobes, C_n. See Fig. 3b. Under the Poincaré map the escape and capture lobes map accordingly: $E_n \mapsto E_{n+1}$ and $C_n \mapsto C_{n+1}$. The critical step in the ionization process is the mapping of the E_{-1} lobe to the E_0 lobe because the E_{-1} lobe is fully contained within the resonance zone while the E_0 lobe lies outside it. This portion of the homoclinic tangle is called a turnstile because it acts as a vehicle to transport electrons from bound to ionized states.

One can gain physical understanding for the turnstile mechanism by following the electron dynamics under application of small delta function (i.e., instantaneous) kicks to an electron. In the absence of kicks, electron trajectories are characterized by the sign of their energy. Electrons with negative energy are bound while electrons

with positive energy are free. The zero energy orbit forms a separatrix, which separates these bound and free regions of phase space. This simple unkicked system can be studied using the Poincaré return map introduced above, with the understanding that the Poincaré map is now equivalent to strobing the system at regular intervals of period T. As long as the ratio of the electron's classical Kepler period to the strobing period is not a rational number, iterates of the Poincaré map generate a sequence of points in phase space that, after many iterations, fills in the trajectory curve from the continuous phase space evolution. Applying the alternating delta function kicks to this system causes the separatrix to split into stable and unstable manifolds. The initial portion of the unstable manifold, with negative momentum, closely follows the lower branch of the separatrix in the unkicked system (Fig. 3b). (Similarly the initial portion of the stable manifold, with positive momentum, closely follows the upper branch of the unkicked separatrix.) Intersections between the stable and unstable manifolds occur every integer multiple of half the kicking period. For example, taking the first intersection to be at the nucleus (with infinite momentum, see Fig. 3b), the second intersection closest to the nucleus, with negative momentum, is $T/2$ away from the nucleus. The third intersection is T away from the nucleus, the fourth $3T/2$, and so on.

We now focus on the electron trajectory whose (initially bound) phase space position before the applied ionization kicks is near the unkicked separatrix, just above the unstable manifold and inside the E_{-1} lobe. The first step in the map is to apply half of the positive kick to the electron. This step makes the electron momentum less negative and hence the electron orbit becomes more bound. The next step in the map is to let the electron evolve freely for $T/2$. Since the orbit has negative momentum, the electron is moving towards the nucleus, and since we are assuming small deviations from the separatrix, this orbit closely follows the separatrix. After $T/2$ it is still moving towards the nucleus and is positioned somewhere above the C_0 lobe. The third step in the map is to apply the full negative kick. This step ionizes the orbit since the electron is "pushed" to just below the separatrix. The fourth step in the map is to again let the electron evolve freely for $T/2$. The electron continues moving towards the nucleus, but after $T/2$ it has bounced off the nucleus and emerged with positive momentum. However, since its orbit is now unbound, after $T/2$ the electron is above the separatrix in phase space. Hence the application of the final half of the positive kick only increases the electron momentum and the orbit remains unbound. Hence the bound orbit from inside the E_{-1} lobe maps to an unbound orbit inside the E_0 lobe. One can apply the same reasoning to understand how the rest of the lobes map into each other.

All electron trajectories that are inside the E_{-1} lobe ionize after a single application of the map, whereas trajectories just outside the E_{-1} lobe require further applications of the map before ionization occurs. [16] Hence
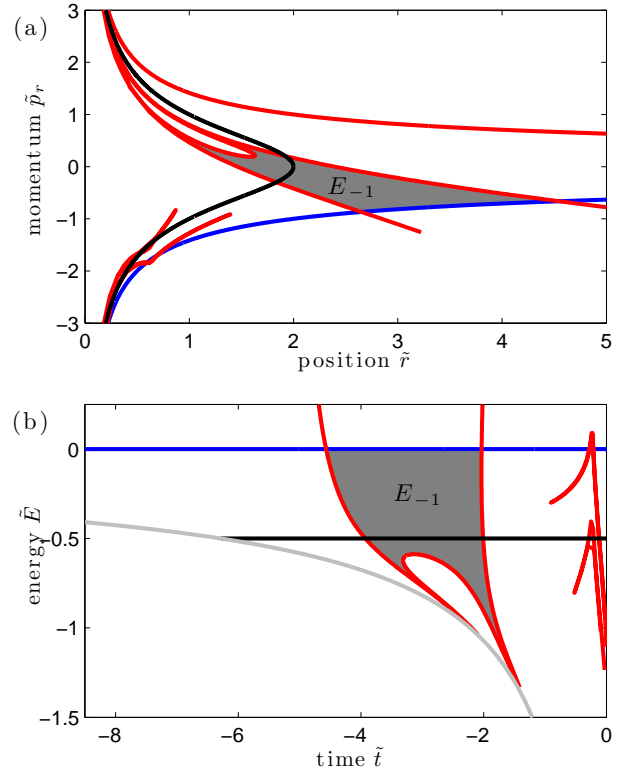

FIG. 4: The turnstile in physical and energy-time coordinates. The starting energy shell is represented by the red line. The energy axis is labeled in scaled units and $\tilde{t} = 2\pi$ corresponds to the Kepler period. The system parameters used in creating these figures are chosen for pedagogical reasons and do not correspond to parameters used to generate experimental or numerical results.

only that portion of an energy shell that overlaps the E_{-1} lobe is ionized after application of the pulse sequence shown in Fig. 2a. Figure 4a shows the E_{-1} lobe together with a line representing the initial energy shell, i.e., the locus of points in phase space that correspond to the energy $\tilde{E} = -1/2$.

To better understand how the overlap between the energy shell and the E_{-1} lobe, and hence the ionization fraction, changes as the kick strength $\Delta \tilde{p}$ and the kicking period T are varied, a canonical set of energy-time coordinates is introduced. The energy coordinate $\tilde{E}$ is the electron energy, and the time coordinate $\tilde{t}$ is the negative time it takes the electron to reach the nucleus. The turnstile lobe in these coordinates is shown in Fig. 4b. The light gray curve is the phase-space boundary defined by the negative Kepler period $-\tilde{T}_k$ of each energy $\tilde{E}$. This curve is physically identified with the right vertical boundary at $\tilde{t} = 0$, i.e., both the gray curve and the vertical line at $\tilde{t} = 0$ represent an electron striking the nucleus. Time evolution in these coordinates consists of uniform motion from left to right along horizontal lines. When a trajectory reaches $\tilde{t} = 0$, it jumps back to $\tilde{t} = -\tilde{T}_k$.
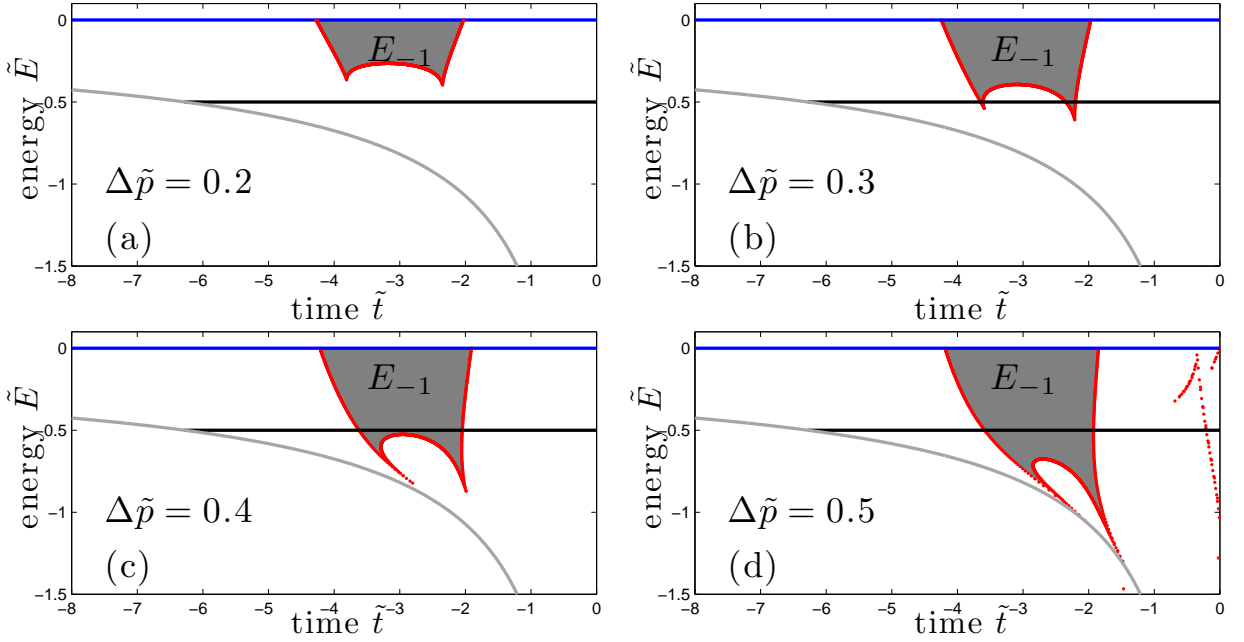
FIG. 5: E_{-1} lobe characteristics in energy-time coordinates for $T = 3$ns and the kick strengths $\Delta\tilde{p}$ indicated.

The E_{-1} lobe has two long "horns". In energy-time coordinates these horns stretch downward until they reach the left phase space boundary and then re-emerge on the right boundary, only this time stretching upwards. Hence, in the example chosen (Fig. 4b), the E_{-1} lobe overlaps the energy shell (the thick black line) in one broad interval together with two narrow intervals associated with the horns that wrap around the nucleus. The fraction of the energy shell that overlaps the E_{-1} lobe, and hence the ionization fraction, thus corresponds to the fraction of time a trajectory of energy $\tilde{E} = -1/2$ spends inside the E_{-1} lobe. This can be calculated by dividing the total length of the line of constant energy lying within the E_{-1} lobe by the scaled Kepler period 2π.

V.   ROLE OF THE TURNSTILE GEOMETRY

A.   Small T

We first consider the turnstile geometry for values of T roughly equal to or less than the Kepler period $T_k = 4.35$ns. We pay particular attention to how the geometry changes as a function of the kick strength $\Delta\tilde{p}$. Figure 5 shows the E_{-1} lobe in energy-time coordinates for increasing values of $\Delta\tilde{p}$ and a fixed value of $T = 3$ns. For small values of $\Delta\tilde{p}$ there is no overlap between the E_{-1} lobe and the energy shell (Fig. 5a), whereupon the ionization fraction is zero. As $\Delta\tilde{p}$ increases the splitting between the stable (red) and the unstable (blue) manifolds increases and elongates the E_{-1} lobe while keeping the positions of the intersections between the stable and unstable manifolds unchanged. The horns cross the en-

ergy shell at some critical value $\Delta\tilde{p}_i$ (Fig. 5b), whereup the ionization fraction becomes nonzero. Since the horn tips are very narrow, the ionization fraction initially remains close to zero. As $\Delta\tilde{p}$ increases the horns elongate further and the overlap with the energy shell broadens leading to a rapid increase in the ionization fraction. At a critical value of $\Delta\tilde{p}_s$ the main body of the E_{-1} lobe begins to overlap the energy shell; the two "horn" intervals merge into a single interval (Fig. 5c). Further increases in $\Delta\tilde{p}$ increase the length of the E_{-1} lobe but do not significantly increase the overlap between the E_{-1} lobe and the energy shell (Fig. 5d). As a result, further increase in the ionization fraction is slow, leading to the shoulder seen in Fig. 6. This progression was explained in Ref. [12], Sec. 4B, and leads to the steep increase followed by a plateau in the ionization fraction.

Appendix A derives two approximations to f for small values of $\Delta\tilde{p}$. See Fig. 6. The first approximation is for delta-function kicking

$$f = \frac{32}{3\pi}\Delta\tilde{p}^3. \tag{2}$$

Though this is an overestimate, it nevertheless follows the initial rise. It is also independent of the kicking period T. However, it displays a gradual growth from zero, without the critical kick strength $\Delta\tilde{p}_0 \approx 0.25$.

The second approximation is more accurate and allows for the small nonzero width of the kicking pulses. [See Eqs. (A12) and (A13).] Figure 6 shows that this approximation more accurately matches the initial rise of f than the first approximation. It yields an initial critical value
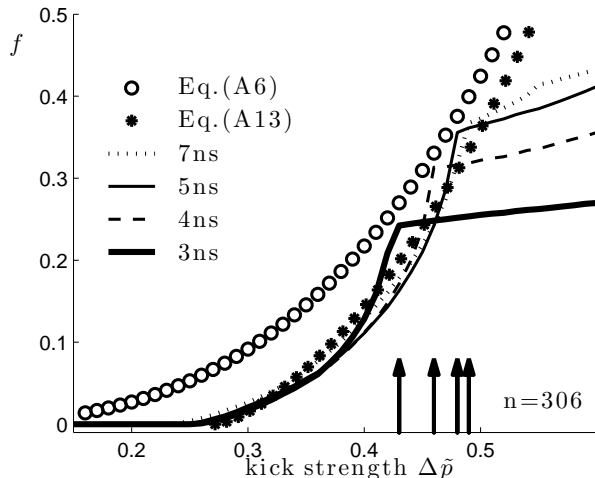
FIG. 6: Ionization fraction as a function of kick strength $\Delta\tilde{p}$. The lines represent the classical trajectory Monte Carlo simulations for $T = 3$, 4, 5, and 7ns ($n = 306$). Arrows mark positions of the shoulders for each of the data series.

of the kick strength

$$\Delta\tilde{p}_0 = \left(\frac{\tilde{\tau}_k}{36}\right)^{1/3} \approx 0.27. \qquad (3)$$

The last step follows from the fact that the kick duration $\tau_k = 500$ps is equal to $\tilde{\tau}_k = 0.72$ in scaled atomic units (for $n = 306$). This closely matches the initial onset seen in Fig. 6. Finally, the second approximation is also independent of T, thus providing an explanation for the universal form in the rise of f as a function of $\Delta\tilde{p}$. We have therefore theoretically explained why the initial rise is independent of T and have provided an accurate theoretical value for the critical kicking strength.

Using a Melnikov analysis (similar to that in Appendix A), Ref. [12] showed that the shoulder occurs at $\Delta\tilde{p}_{\text{shoulder}} = 0.285\tilde{T}^{1/3}$. The quantity $\Delta\tilde{p}_{\text{shoulder}}$ is shown for different values of T by the vertical lines in Fig. 6. For $T = 5$ns it yields the value $\Delta\tilde{p}_{\text{shoulder}} = 0.55$ which is half way between the experimental value (0.6) and the numerical value (0.5) .

The separation and ordering of the $T = 5, 7, 9$ns data (Fig. 1b) after the shoulder can be understood in terms of the overall widths of the turnstile lobes in Fig. 5. It was demonstrated in Ref. [12] that the widths of the lobes scale linearly in T. Thus, we should expect the larger T values to have larger ionization fractions, after the shoulder, as in Figures 1b and 1c.

B. Large T

The same analysis can be repeated for larger values of T. Figure 7 shows the behavior of the E_{-1} lobe for the same values of $\Delta\tilde{p}$ as used in Fig. 5 but for $T = 11$ns. The intersections between the E_{-1} lobe and the energy shell

now occur farther to the left and the width of the E_{-1} lobe is substantially increased [12]. As in Fig. 5, for small values of $\Delta\tilde{p}$ there is no overlap between the E_{-1} lobe and the energy shell, and the ionization fraction is zero. However, as $\Delta\tilde{p}$ increases and the E_{-1} lobe elongates the left and right horns behave differently. The left horn is being "squeezed" against the phase space boundary and becomes narrower than the right one. The result of this squeezing is a change in the "angle" between the boundary of the E_{-1} lobe and the energy shell which becomes more obtuse as T increases. Hence the overlap between the turnstile and the energy shell continues to increase even after the energy shell overlaps the main portion of the lobe.

As T becomes much larger than the Kepler period, the ionization fraction as a function of $\Delta\tilde{p}$ comes to be independent of T as illustrated in Fig. 8. This could be understood as follows. The first positive kick in the ionization sequence transforms the ensemble from a single energy shell to a distribution of energy shells. (In the limit of delta function kicks, the energy follows a square Lorentzian distribution.) Note that the ensemble of electron trajectories is not uniformly distributed in time along the Kepler orbits. However, as time after the kick increases, the ensemble redistributes itself along the Kepler orbits, eventually leading to a distribution that is approximately stationary. Once $T/2$ is large enough to reach this steady state (i.e. $T/2$ much greater than the Kepler period 4.35 ns), any further increase in T has no effect on the electron distribution when the second pulse arrives. A similar steady state is obtained in the interval between the second and third pulses. Thus the ionization fraction itself becomes independent of T. Appendix B derives an approximation for the ionization fraction f based on this approach. (See Fig. (9).) Note that there is no shoulder in this approximation, consistent with the experimental and computational data in Figs. 1 and 2.

We now consider what happens to the turnstile lobe geometry at large T. The lobes are further sheered in the energy-time phase space and are forced to "wrap around" the nucleus. The lobe will have numerous small intersections with the energy shell, creating an approximately uniform distribution. At this point, this distribution becomes more important than the overall geometry of the turnstile.

VI. CONCLUSIONS

We have demonstrated the important role played by a phase-space turnstile in governing the chaotic ionization of quasi-1D Rydberg atoms, driven by a train of alternating kicks. Only the portion of the energy shell overlapping the turnstile ionizes during a single kicking cycle. In particular, we investigated the dependence of the ionization fraction on the kick strength and the duration of the kicking cycle.
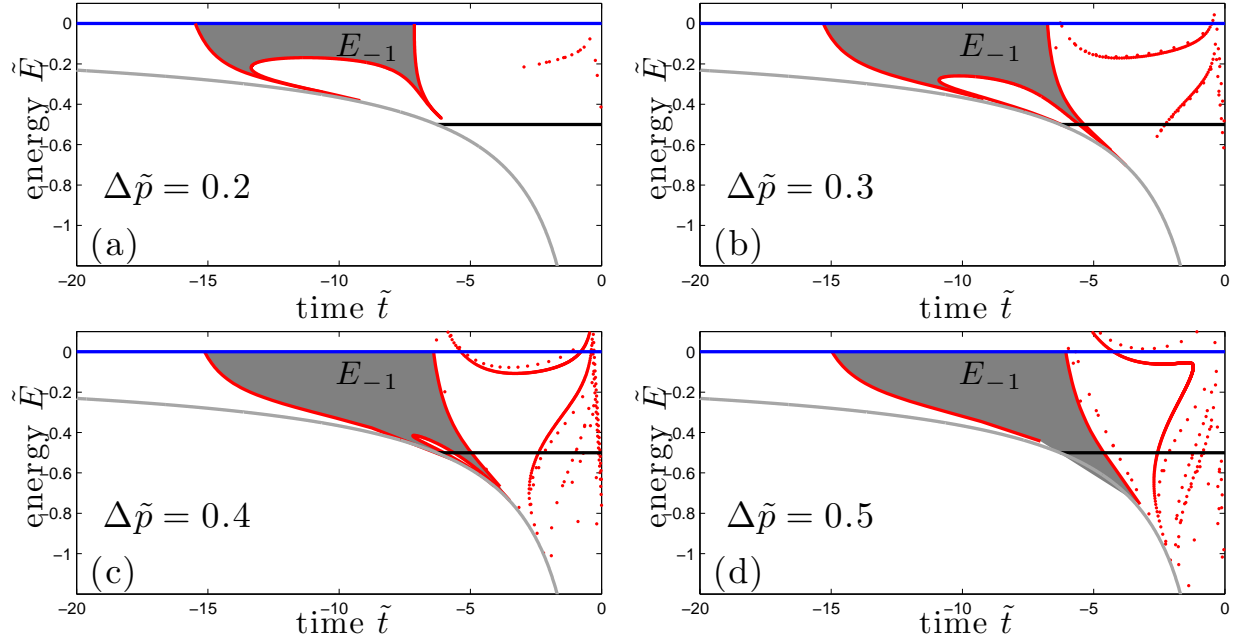
FIG. 7: E_{-1} lobe characteristics in energy-time coordinates for $T = 11$ns and the kick strengths $\Delta\tilde{p}$ indicated.
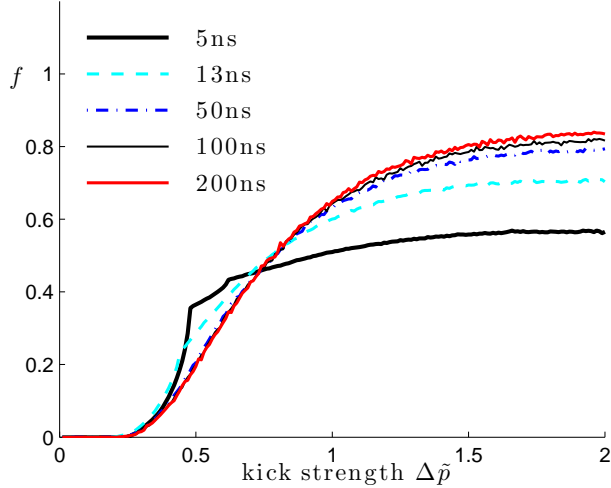

FIG. 8: Ionization fraction as a function of kick strength $\Delta\tilde{p}$ for the values of T indicated.
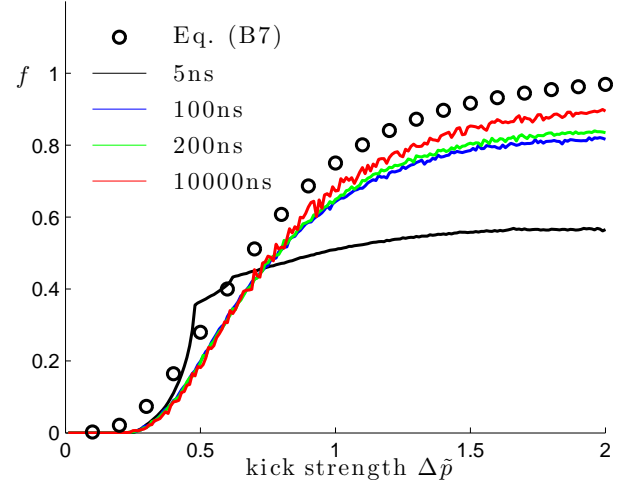

FIG. 9: Ionization fraction as a function of kick strength $\Delta\tilde{p}$.

More broadly, the data demonstrate that alternating pulse sequences can generate turnstiles that transport electrons from one localized region of phase space to a new localized region of phase space. With appropriately designed pulse amplitudes and timing this might be exploited to capture free electrons into bound states, to rapidly transport localized wave packets between different regions of phase space, i.e., to induce "hopping" to a narrow distribution of final energy states, and (by systematically varying the position of the turnstile lobe) to map the phase space distribution associated with a diffuse initial wave packet.

Appendix A: Ionization fraction f for small $\Delta\tilde{p}$

We derive the dependence of the ionization fraction f on the scaled kicking strength $\Delta\tilde{p}$, when $\Delta\tilde{p}$ is small. This dependence is shown to be independent of the scaled kicking period $\tilde{T}$.
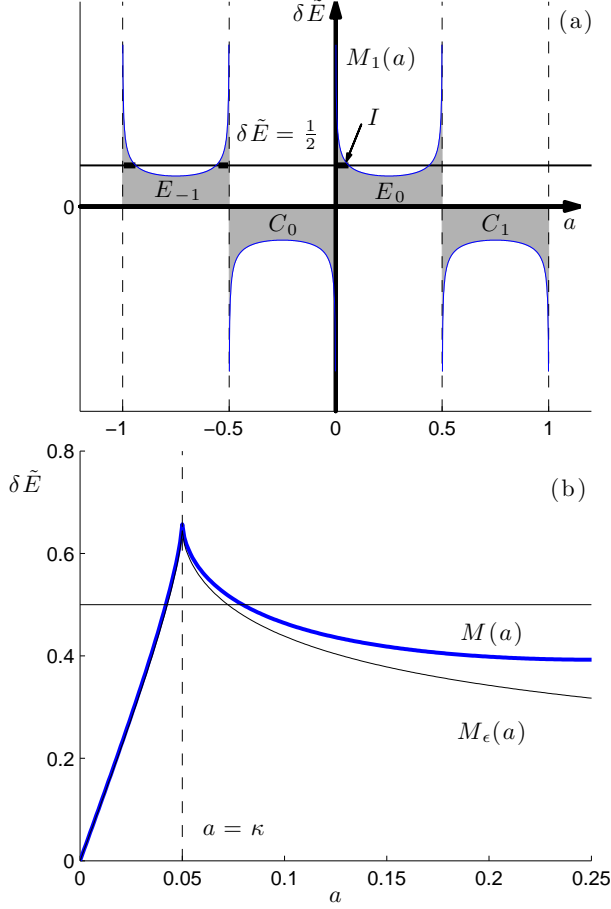
1. Delta-function kicking

FIG. 10: (a) The approximation $M_1(a)$ to the Melnikov function $M(a)$ appropriate for delta-function kicking. (b) The Melnikov function $M(a)$ for square wave kicking with nonzero width. Parameters used in both figures are $T = 5$ns, $\Delta\tilde{p} = 0.35$, and $\tau_k = 500$ps.

We use the Melnikov function M [2, 17], computed in Ref. [12], which measures the splitting between the stable and unstable manifolds. More precisely, in the limit of small kick strength $\Delta\tilde{p}$, the stable and unstable manifolds may be viewed as perturbations to the unkicked separatrix at $\tilde{E} = 0$. Denoting the time along the separatrix by $\tilde{t}$ (with $\tilde{t} = 0$ at the nucleus), $M(\tilde{t})$ is the difference in energy $\tilde{E}$ between the unstable and stable manifolds, perturbed away from point $\tilde{t}$ along the separatrix.

In Ref. [12], Eq. (B10), the Melnikov function is com-

puted as a function of $a = \tilde{t}/\tilde{T}$ to be

$$M(a) = \frac{\Delta\tilde{p}}{2\kappa\tilde{T}^{1/3}}\left(\frac{9}{2}\right)^{1/3} \times \tag{A1}$$

$$\sum_{n\in\mathbb{Z}}\Big[|a+n+\kappa|^{2/3} - |a+n-\kappa|^{2/3}$$

$$-|a+n+1/2+\kappa|^{2/3} + |a+n+1/2-\kappa|^{2/3}\Big],$$

where $\kappa = \tilde{\tau}_k/(2\tilde{T})$ [18]. For small values of κ, i.e. for short kicking pulses, Eqs. (B14) and (B15) in Ref. [12] demonstrate that

$$M(a) = M_1(a) + O\left(\frac{\kappa^2}{\delta a^{4/3}}\right), \tag{A2}$$

$$M_1(a) = \frac{\Delta\tilde{p}}{\tilde{T}^{1/3}}\left(\frac{4}{3}\right)^{1/3} \times$$

$$\sum_{n\in\mathbb{Z}}\left[\frac{|a+n|^{2/3}}{a+n} - \frac{|a+n+1/2|^{2/3}}{a+n+1/2}\right], \tag{A3}$$

where δa $(-1/4 \le \delta a \le 1/4)$ is the distance of a to the nearest integer or half-integer.

For delta-function kicks, κ goes to 0 so that the error term in Eq. (A2) vanishes and the Melnikov function is simply $M_1(a)$. Fig. 10a shows $M_1(a)$. The regions between the graph of $M_1(a)$ and the horizontal axis represent the capture and escape lobes. The escaping flux f after one iterate is then proportional to the intersection length between E_{-1} and the line $\delta\tilde{E} = 0.5$, which represents the initial electron state. As evident from the translational and reflection symmetry of $M_1(a)$ shown in Fig. 10a, the intersection between E_{-1} and the line $\delta\tilde{E} = 0.5$ equals twice the length of the shifted interval I in Fig. 10a. Since the length ℓ_I of I is small (justified below), it may be computed by assuming $0 < a \ll 1$ in Eq. (A3), yielding

$$M_1(a) = \frac{\Delta\tilde{p}}{\tilde{T}^{1/3}}\left(\frac{4}{3}\right)^{1/3}\frac{1}{a^{1/3}}. \tag{A4}$$

Setting $M_1(a) = 1/2$ yields

$$\ell_I = \frac{32\Delta\tilde{p}^3}{3\tilde{T}}. \tag{A5}$$

Since ℓ_I is proportional to $\Delta\tilde{p}^3$, we have justified our above assertion that ℓ_I is small. Multiplying ℓ_I by $2\tilde{T}$ and dividing by the scaled period 2π yields the ionization fraction

$$f = \frac{2\tilde{T}\ell_I}{2\pi} = \frac{32}{3\pi}\Delta\tilde{p}^3. \tag{A6}$$

This approximation is shown as the open circles in Fig. 6. It is an overestimate of the ionization fraction computed by classical trajectory Monte Carlo (CTMC) simulations, which are shown in Fig. 6 for different values of $\tilde{T}$. Nevertheless, this approximation does reflect the fact that at small values of $\Delta\tilde{p}$, the ionization fraction f is independent of $\tilde{T}$.

2. Square-wave kicking

A more accurate approximation to the initial rise of the ionization fraction as a function of $\Delta\tilde{p}$ is computed by acounting for the width $\tilde{\tau}_k$ of the kicking pulses. Most importantly, when $\kappa = \tilde{\tau}_k/(2\tilde{T})$ is nonzero, we must properly model the horn of $M(a)$ in Fig. 10b. Equation (A1) shows that the horn (i.e., the discontinuity in dM/da) occurs at $a = \kappa$. The height of the horn is then $M(\kappa)$. To lowest order in κ, Eq. (A1) yields

$$M(\kappa) = \Delta\tilde{p}\left(\frac{9}{4\kappa\tilde{T}}\right)^{1/3} + O(\kappa^0). \tag{A7}$$

If the height of the horn is less than the scaled energy $1/2$, then there is no ionization. The critical momentum $\Delta\tilde{p}_0$ at which ionization first occurs is thus approximated by setting $M(\kappa) = 1/2$ in Eq. (A7) and solving for $\Delta\tilde{p}$ to lowest order in κ, yielding

$$\Delta\tilde{p}_0 = \left(\frac{\kappa\tilde{T}}{18}\right)^{1/3} = \left(\frac{\tilde{\tau}_k}{36}\right)^{1/3}. \tag{A8}$$

Thus, $\Delta\tilde{p}_0$ is independent of the kicking period $\tilde{T}$. This explains why the initial onset of f observed in Fig. 2b is independent of $\tilde{T}$.

To compute the initial rise of f, we set $\epsilon = a - \kappa$ in Eq. (A1)

$$M(a) = \frac{\Delta\tilde{p}}{2\kappa\tilde{T}^{1/3}}\left(\frac{9}{2}\right)^{1/3} \times \tag{A9}$$
$$\sum_{n\in\mathbb{Z}}\left[|\epsilon + n + 2\kappa|^{2/3} - |\epsilon + n|^{2/3}\right.$$
$$\left. -|\epsilon + n + 1/2 + 2\kappa|^{2/3} + |\epsilon + n + 1/2|^{2/3}\right].$$

Taking ϵ and κ to be the same order, i.e. $O(\epsilon) = O(\kappa)$, the terms $|\epsilon + 2\kappa|^{2/3} - |\epsilon|^{2/3}$ in the sum are order $\epsilon^{2/3}$. All other terms in the sum are order ϵ or higher. So, to lowest order in ϵ,

$$M(a) = M_\epsilon(a) + O(\epsilon), \tag{A10}$$

where the approximation M_ϵ is

$$M_\epsilon(a) = \frac{\Delta\tilde{p}}{2\kappa\tilde{T}^{1/3}}\left(\frac{9}{2}\right)^{1/3}\left(|\epsilon + 2\kappa|^{2/3} - |\epsilon|^{2/3}\right)$$
$$= \frac{\Delta\tilde{p}}{2\kappa\tilde{T}^{1/3}}\left(\frac{9}{2}\right)^{1/3}\left(|a + \kappa|^{2/3} - |a - \kappa|^{2/3}\right). \tag{A11}$$

Re-expressing the argument of $M_\epsilon(a)$ in terms of $\tilde{t} = a\tilde{T}$,

$$M_\epsilon(\tilde{t}) = \frac{\Delta\tilde{p}}{\tilde{\tau}_k}\left(\frac{9}{2}\right)^{1/3}\left(|\tilde{t} + \tilde{\tau}_k/2|^{2/3} - |\tilde{t} - \tilde{\tau}_k/2|^{2/3}\right). \tag{A12}$$

The interval I in Fig. 10c is thus bounded by $\tilde{t}_L$ and $\tilde{t}_R$ obtained by solving $M(\tilde{t}) = 1/2$, which is done numerically. The ionization fraction is then

$$f = \frac{2(\tilde{t}_R - \tilde{t}_L)}{2\pi}. \tag{A13}$$

Note that since $M(\tilde{t})$ does not depend on $\tilde{T}$, for a fixed value of $\tilde{\tau}_k$, the roots $\tilde{t}_L$ and $\tilde{t}_R$ also do not depend on $\tilde{T}$. Hence the initial rise of f does not depend on $\tilde{T}$, as seen in the CTMC simulations in Fig. 6. Approximation (A13) is shown as the solid dots in Fig. 6. Note the excellent agreement with the initial rise of f, regardless of $\tilde{T}$. For each value of $\tilde{T}$, f eventually deviates from Eq. (A13) and forms the shoulder. In Ref. [12], Eq. (B20), it was shown that this shoulder occurs at $\Delta\tilde{p} = 0.285\tilde{T}^{1/3}$. In Fig. 6, these shoulder values are denoted by the vertical lines, nicely matching the CTMC data.

Appendix B: Ionization fraction f for large $\tilde{T}$

We now present a method to approximate the ionization fraction for large $\tilde{T}$ that does not explicitly depend on the turnstile structure. The initial electron state is described by an invariant classical distribution restricted to the energy shell $\tilde{E} = -1/2$.

$$\tilde{E}_0 = \frac{\tilde{p}^2}{2} - \frac{1}{\tilde{r}} = -\frac{1}{2}. \tag{B1}$$

In momentum space the distribution $\rho(\tilde{p})$ is symmetric about and peaked at $\tilde{p} = 0$. The flux $\Phi(\tilde{p}) = \rho(\tilde{p})d\tilde{p}/d\tilde{t}$ through $\tilde{p}$ is constant for all values of $\tilde{p}$. Hence,

$$\Phi(\tilde{p}) = \rho(\tilde{p})\frac{d\tilde{p}}{d\tilde{t}} = -\rho(\tilde{p})\left(\frac{\tilde{p}^2}{2} - \tilde{E}_0\right)^2 = -A_0, \tag{B2}$$

where A_0 is a normalization constant.

Imparting a kick changes the shape of this distribution. Here we assume delta-function kicks which impart the same total impulse $\Delta\tilde{p}$ as the kicks shown in Fig. 2a. A delta-function kick changes the energy of the electron by

$$\Delta\tilde{E} = \frac{2\tilde{p}\Delta\tilde{p} + \Delta\tilde{p}^2}{2}. \tag{B3}$$

Since the change in energy depends on the electron's initial momentum, we are now able to write down the distribution of energy change for the electron ensemble as a result of a single kick.

$$\rho(\Delta\tilde{E}) = \frac{4A_0|\Delta\tilde{p}|^3}{\left[\left(\Delta\tilde{E} - \frac{\Delta\tilde{p}^2}{2}\right)^2 - 2\Delta\tilde{p}^2\tilde{E}_0\right]^2}. \tag{B4}$$

The energy distribution is then given by

$$\rho_f(\tilde{E}_f) = \frac{4A_0|\Delta\tilde{p}|^3}{\left[\left(\tilde{E}_f - \tilde{E}_0 - \frac{\Delta\tilde{p}^2}{2}\right)^2 - 2\Delta\tilde{p}^2\tilde{E}_0\right]^2}$$
$$\equiv G(\tilde{E}_f; \tilde{E}_0, \Delta\tilde{p}). \tag{B5}$$

This is the final energy distribution resulting from a single kick imparted to an initial stationary ensemble with energy $\tilde{E}_0$. In the general case of an arbitrary initial stationary ensemble, with energy distribution $\rho_i(\tilde{E}_i)$, the final energy distribution is

$$\rho_f(\tilde{E}_f) = \int d\tilde{E}_i \ \rho_i(\tilde{E}_i)G(\tilde{E}_f; \tilde{E}_i, \Delta\tilde{p}). \qquad \text{(B6)}$$

After the initial kick, the electron ensemble has the energy distribution Eq.(B5), with $\tilde{E}_0 = -1/2$. This ensemble is not stationary. However, as time evolves after the initial kick, the electron trajectories increasingly "randomize" their positions along the time-axis, due to the variation in Kepler periods. At sufficiently long times (relative to the Kepler periods), the ensemble will thereby reach an approximate steady state. Thus, for large values of $\tilde{T}$, the energy distribution resulting from the second (and third) kick is obtained by Eq.(B6). Putting all three kicks together, we obtain

$$\rho(\tilde{E}_{f_3}) = \int d\tilde{E}_{f_2} G\left(\tilde{E}_{f_3}; \tilde{E}_{f_2}, \frac{\Delta\tilde{p}}{2}\right) \int d\tilde{E}_{f_1} G\left(\tilde{E}_{f_2}; \tilde{E}_{f_1}, -\Delta\tilde{p}\right) G\left(\tilde{E}_{f_1}; -\frac{1}{2}, \frac{\Delta\tilde{p}}{2}\right), \qquad \text{(B7)}$$

where n in $\tilde{E}_{f_n}$ denotes the energy distribution after the n-th kick. (Note that the kick imparted during the first and last kick is half the size and in a different direction than the second kick.)

The ionization occurs when the final electron energy is positive. This yields the approximation shown in Fig. 9. Even though this approach overestimates the ionization fraction, it does capture the essential features for large T. (Note that the excess ionization fraction is a consequence of the delta-function approximation to the kicks.) In particular, this approximation does not depend on T and thus we have shown that for large T the overall shape of the ionization fraction is independent of T.

[1] S. Wiggins, *Chaotic Transport in Dynamical Systems* (Springer-Verlag, New York, 1992).
[2] J. Guckenheimer and P. Holmes, *Nonlinear Oscillations, Dynamical Systems, and Bifurcations of Vector Fields* (Springer-Verlag, New York, 2002).
[3] A. M. Selvam, *Chaotic Climate Dynamics* (Luniver Press, 2007).
[4] T. H. Solomon, S. Tomas, and J. L. Warner, Phys. Rev. Lett. **77**, 2682 (1996).
[5] G. A. Voth, G. Haller, and J. P. Gollub, Phys. Rev. Lett. **88**, 254501 (2002).
[6] S. C. Shadden, J. O. Dabiri, and J. E. Marsden, Physics of Fluids **18**, 047105 (2006).
[7] L. Glass and M. C. Mackey, *From Clocks to Chaos: The Rhythms of Life* (Princeton University Press, 1988).
[8] W. Zhao, J. J. Mestayer, J. C. Lancaster, F. B. Dunning, C. O. Reinhold, S. Yoshida, and J. Burgdörfer, Phys. Rev. Lett. **97**, 253003 (2006).
[9] R. Blümel and W. P. Reinhardt, *Chaos in atomic physics* (Cambridge University Press, Cambridge, United Kingdom, 1997).
[10] K. Burke, K. A. Mitchell, B. Wyker, S. Ye, and F. B. Dunning, Phys. Rev. Lett. **107**, 113002 (2011).
[11] F. B. Dunning, J. J. Mestayer, C. O. Reinhold, S. Yoshida, and J. Burgdörfer, J. Phys. B: At. Mol. Opt. Phys. **42**, 022001 (2009).
[12] K. Burke and K. A. Mitchell, Phys. Rev. A **80**, 033416 (2009).
[13] K. A. Mitchell, J. P. Handley, B. Tighe, A. Flower, and J. B. Delos, Phys. Rev. Lett. **92**, 073001 (2004).
[14] K. A. Mitchell, J. P. Handley, B. Tighe, A. Flower, and J. B. Delos, Phys. Rev. A **70**, 043407 (2004).
[15] T. Topcu and F. Robicheaux, J. Phys. B **40**, 1925 (2007).
[16] A slight difference exists between the turnstile defined for periodic forcing (Fig. 3) and that defined for a single forcing cycle as in the experiment (Fig. 4). See also Ref. [19].
[17] V. K. Melnikov, Trans. Mosc. Math. Soc. **12**, 1 (1963).
[18] Note that the same notation M is used for the Melnikov function, whether it's argument is $\tilde{t}$ or $a = \tilde{t}/\tilde{T}$.
[19] B. Mosovsky and J. Meiss, SIAM J. Dyn. Sys. **10**, 35 (2011), http://dx.doi.org/10.1137/100794110.